Surface Forces and Stratification in Foam Films Formed with Bile Salts

Journal:	*Molecular Systems Design & Engineering*
Manuscript ID	ME-ART-02-2020-000024.R1
Article Type:	Paper
Date Submitted by the Author:	14-May-2021
Complete List of Authors:	Yilixiati, Subinuer; University of Illinois at Chicago, Department of Chemical Engineering Uribe Ortiz, Camila; University of Illinois at Chicago, Department of Chemical Engineering Sharma, Vivek; University of Illinois at Chicago, Department of Chemical Engineering

Surface Forces and Stratification in Foam Films Formed with Bile Salts

Subinuer Yilixiati, Camila Alexandra Uribe Ortiz, and Vivek Sharma

Chemical Engineering, University of Illinois at Chicago, IL.

Submitted on February 18th, 2020; Revised on May 13th, 2021

Address correspondence to: viveks@uic.edu

Abstract: Bile salts, especially in their aggregated or micellar form, play a critical role in health and medicine by solubilizing cholesterol, fat-soluble vitamins, and drugs. However, in contrast to the head-tail (HT) surfactants like sodium dodecyl sulfate (SDS), amphiphilic bile salts have an unusual steroid structure and exhibit a smaller aggregation number (N_{agg} < 20 molecules per micelle vs. N_{agg} > 50 for SDS). Foam films formed by micellar solutions of typical surfactants like SDS exhibit stratification manifested as stepwise thinning and coexistence of flat thick-thin regions that differ by a step-size proportional to the intermicellar distance. We consider drainage *via* stratification studies as an effective and insightful probe of the strength and magnitude of intermicellar interactions and resulting supramolecular oscillatory structural (SOS) surface force contribution to disjoining pressure. However, there are neither prior reports of stratification in foam films formed with bile salt solutions nor measurements of SOS surface forces. Here we report the discovery and characterization of stratification in foam films formed by aqueous solutions of four bile salts – sodium cholate (NaC), sodium taurocholate (NaTC), sodium deoxycholate (NaDC), and sodium glycodeoxycholate (NaGDC) – that have a similar steroid nucleus, but difference in conjugation sites and the number of hydroxyl groups (3 for NaC and NaTC, 2 for NaDC and NaGC). Using IDIOM (Interferometry Digital Imaging Optical Microscopy) protocols we developed recently to characterize and analyze thickness variations and transitions, we find that foam films made with bile salts exhibit fewer stepwise transitions and smaller step-size than SDS solutions. Also, we measured a lower drop in surface tension and lower magnitude of thickness-dependent disjoining pressure compared to SDS solutions. We find that the bile salts with a matched number of hydroxyl groups exhibit similar properties in tensiometry and foam film studies. We show that the stratification studies can characterize the influence of chemical structure on the magnitude and range of intermicellar interactions as well their influence on drainage and stability of foam films.

Design, system and applications

Commonly used soaps or detergents and biological lipids are head-tail (HT) surfactants that consist of relatively flexible, long one or two hydrophobic tail(s) (8-20 carbon chain) and a highly hydrophilic head. In contrast, the amphiphilic bile salts consist of a rigid heterocyclic steroid nucleus with limited separation of hydrophobic and hydrophilic regions, leading to imperfect-packing within highly polydisperse aggregates, have smaller size and lower stability compared to HT surfactants. Due to the critical role of micelles of bile salts in health and medicine, understanding the influence of chemical structure differences on their self-assembly and intermicellar interactions constitutes an essential step towards molecular engineering biosurfactants and pharmaceuticals. We report the first evidence of drainage *via* stratification of micellar foam films formed with bile salts in this contribution. We analyze the nanoscopic stepwise thickness transitions and surface forces using IDIOM protocols we developed recently. Lastly, we present stratification studies as an efficient, elegant, cost-effective, and quantitative probe for the characterization of the strength and range of intermicellar interactions and surface forces, without the need for bespoke instrumentation warranted in structure-based methods like x-ray, neutron, or light scattering, and force-based techniques like AFM or SFA.

INTRODUCTION

The collaborative self-assembly of bile salts, phospholipids, and cholesterols forms mixed micelles that play a critical role in the solubilization of fats and biomolecules (including bilirubin, lecithin, and fat-soluble vitamins in the intestine),[1-11] gall-stone formation or dissolution,[1, 6, 7] cholesterol homeostasis,[8] and drug delivery.[1-14] Though the importance of bile has been known since antiquity, discussed by Hippocrates (460-370 B.C.), Charak (3rd century B.C.), and even Horace (65-8 B.C.; his Ode 1.13 includes the line: "*fervens difficili bile tumet iecur*;" or "my liver swells with bile"), the studies of surfactant-like behavior and self-assembly of bile salts began relatively recently (mid-20th century).[1-4, 7-11, 14, 15] Liver synthesizes salts of bile acids (or "bile salts") from cholesterol, and therefore, bile salts consist of a rigid heterocyclic steroid nucleus containing four saturated rings fused with a convex hydrophobic face. The hydrophilic regions distributed on the concave face include one to three hydroxyl groups and an attached, short flexible chain that is polar.[1-10] Due to their rigid steroidal structure, the amphiphilic bile salts have limited separation of hydrophobic and hydrophilic regions, and imperfect-packing within self-assembled aggregates (referred to as micelles). [1-19] In contrast, commonly used soaps or detergents and foaming agents are head-tail (HT) surfactants that consist of a relatively flexible, long hydrophobic tail (8-20 carbon chain) and a highly hydrophilic head,[20, 21] that self-assembly into micelles with a liquid-like, highly hydrophobic core and a highly hydrophilic shell. Extensive studies probe the surfactant-like properties of bile salts in terms of their micellization and self-assembly, as well as interfacial adsorption and role in the solubilization of fat or drugs.[1-19] However, somewhat surprisingly, the stability and

drainage of foam films containing bile salts (BS) and micelles formed by them have received little or no attention, motivating this study.

The HT surfactants like sodium dodecyl sulfate (SDS) spontaneously self-assemble into micelles with relatively large number of molecules per micelles or large aggregation number, N_{agg} (for SDS, $N_{agg} > 60$) [20, 21] Nearly spherical micelles appear if the bulk concentration of the HT surfactants exceeds the critical micelle concentration (*CMC*), and properties like surface tension show a sharp change in concentration-dependent properties above CMC.[20, 21] In contrast, the micelle core is not entirely hydrophobic for aggregates formed by the bile salts, and concentration-dependent properties like surface tension or conductivity do not reveal a sharp CMC.[1-14] Furthermore, micelles formed by bile salts (or BS micelles) display size polydispersity and smaller aggregate number (N_{agg} ranges from 2 to 15). Micellar foam films formed by the aqueous solutions of HT surfactants like SDS exhibit stratification, manifested as stepwise thinning, and coexistence of flat thick-thin regions that differ by a constant step-size (see Figure 1).[22-34] Thin film interference that leads to the iridescent colors associated with freshly created soap bubbles is also responsible for the thickness-dependent contrast in reflected light intensity of co-existing thick and thin regions below 100 nm[35, 36] (see Figure 1a). By utilizing IDIOM (Interferometry Digital Imaging Optical Microscopy) protocols schematically shown in Figure 1b, we recently developed[29-34] we can quantify thickness transitions and variations accompanying drainage *via* stratification with an exquisite spatio-temporal resolution (thickness ~ 1 nm, in-plane < 1 μm, time < 1ms). For example, the calculation of thickness from the pixel-wise reflected light intensity from each snapshot allows the creation of a nanoscopic thickness map shown in Figure 1a. Thickness variation with time, computed

using the average intensity from a 25 μm side square region at the center of the film plotted in Figure 1c for micellar SDS foams, show that the foam films drain in a stepwise fashion, in agreement with the conventional interferometry-based measurements of average film thickness, as were first reported[37] by Johonnott (1906), and investigated in great detail, primarily in the last three decades. Increasing SDS concentration results in an increase in the number of layers, as shown in Figure 2c for 25 mM and 50 mM SDS foam films.

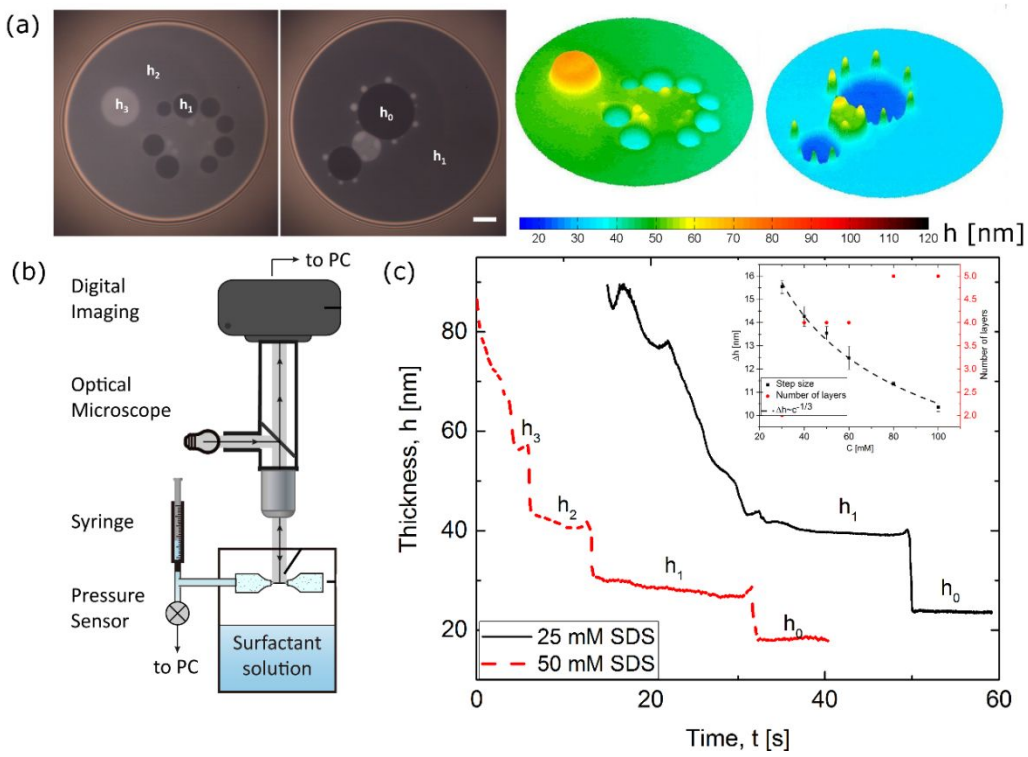

Figure 1. Stratification in micellar foam films of aqueous solutions of sodium dodecyl sulfate (SDS). (a) Two snapshots show stratification in foam film formed with SDS with c = 50 mM SDS ($c/CMC \approx 6$). The corresponding thickness maps are calculated by using the IDIOM (Interferometry Digital Imaging Optical Microscopy) protocols. (b) The schematic shows the IDIOM setup used for visualizing and characterizing drainage *via* stratification. (c) Thickness variation with time is contrasted for micellar foam films formed with c = 25 mM and c = 50 mM, respectively. The data are shifted horizontally for 25 mM SDS ($c/CMC \approx 3$) to illustrate the contrast in step-size, number of steps, and overall drainage kinetics. The inset shows the concentration-dependent variation in step-size and number of steps.

The thickness of freshly formed foam films decreases a monotonically at a rate determined by the influence of capillary stresses, with resistance from bulk and interfacial viscous stresses. However, as drainage in ultrathin foam films (thickness, h < 50 nm) is additionally influenced by disjoining pressure contributed by intermolecular and surface forces that can counterbalance capillary pressure at certain thicknesses.[35, 38-41] In micelle-free films formed with surfactants with c < CMC, the competition between the two pressures leads to the formation of up to two relatively long-lived black films below 25 nm.[35, 38-41] The thickness of Common black film (CBF) is dictated by DLVO forces (named after Derjaguin, Landau, Verwey, and Overbeek) that include both van der Waal forces and electrostatic double layer forces, whereas for in thinner Newton black film (NBF), the shorter range non-DLVO forces like solvation, hydration or steric play critical role.[20, 21, 35, 38, 39, 42] In micellar foam films, the confinement-induced layering of micelles,[22-33, 43, 44] leads to an additional, non-DLVO, but longer-ranged supramolecular oscillatory structural (SOS) contribution to disjoining pressure with alternating attraction-repulsion that leads to stepwise thinning shown in Figure 1c. The step size extracted from the thickness difference between two equilibrium thickness layers far exceeds the dimensions of individual micelles and is presumably comparable to the intermicellar distance. The inset in Figure 1c shows step size varies with a $\Delta h \sim c^{-1/3}$ power law behavior for SDS foam films, emulating the packing behavior of charged spheres and concentration-dependent decrease in intermicellar distance. Each thickness jump represents the formation of one or more thinner, darker domain, and the domains expand at the expense of the thicker surrounding film. In a series of papers, we have demonstrated that domain expansion dynamics,[29, 31] peculiar shapes of non-flat structures visualized using the IDIOM protocols,[30-34] and the thickness

transitions are all sculpted and driven by the supramolecular oscillatory structural surface forces. [29-34] However, after an extensive literature review, we found no reports of stratification studies involving bile salts.

In this contribution, we report the discovery of stratification, including the characterization of step-size and number of stepwise transitions for four distinct bile salts: sodium cholate (NaC), sodium taurocholate (NaTC), sodium deoxycholate (NaDC), and sodium glycodeoxycholate (NaGDC). The four bile salts exhibit differences in the number and position of hydroxyl groups and the conjugation site. We elucidate the impact of distinctive properties of monomeric and self-assembled aggregates of bile salts on adsorption, interactions, and foam stability by complementing the stratification-based studies with thin film balance and tensiometry measurements. We utilize thin film balance and IDIOM protocols to measure the thickness-dependent disjoining pressure of an aqueous solution of one of the bile salts (NaDC). We consider and present these drainage *via* stratification studies as a pragmatic, elegant, (cost-effective), and insightful probe for characterization of the strength and range of intermicellar interactions and surface forces, without the need for bespoke instrumentation needed in structure-based methods like x-ray, neutron, or light scattering, and force-based techniques like AFM or SFA. We anticipate that the comprehesive example of stratification in foam films containing bile salts, these peculiar steroidal surfactants that are important in digestion, pharmaceutical, nutritional, and biomedical research, will inspire researchers to pursue foam film studies for frugal and rapid assesment of chemically-modified analogs as well as for measuring the surface forces, drainage kinetics, and intermicellar distances.

MATERIALS AND METHODS

Bile Salts: Sodium cholate (NaC), sodium taurocholate (NaTC), sodium deoxycholate (NaDC), and sodium glycodeoxycholate (NaGDC): The four bile salts used in this study were purchased from Sigma Aldrich Co., St. Louis, MO and used without further purification. Sodium choate (NaC) is one of the primary bile salts that contribute 80% of the human bile salt fraction, together with sodium chenodeoxycholate (NaCDC),[11] that is not investigated here. We contrast the behavior of NaC (that contains three hydroxyl groups) against the behavior of two secondary bile salts: sodium deoxycholate (NaDC) and sodium glycodeoxycholate (NaGDC), with two hydroxyl groups each. NaDC forms when NaC loses one hydroxyl group through the action of bacterial enzymes, whereas NaGDC forms when NaDC conjugates with glycine. Sodium taurocholate (NaTC), another bile salt with three hydroxyl groups, forms by conjugation of NaC with taurine. The molecular weights and purity of the four as-received bile salt samples are as follows: NaC (M_w = 430.55 Da, >99%), NaTC (M_w = 537.68 Da, >97%), NaDC (anionic, M_w = 414.55 Da, > 97%), and NaGDC (M_w = 471.61 Da, > 97%).

All the solutions were prepared with deionized water, and studies of drainage *via* stratification were carried out primarily with solutions above their nominal critical micelle concentration (CMC). The concentration of bile salts in the gallbladder varies from 10 mM to 50 mM and in the gall capillaries ~5 mM. Although we focus on concentrations of bile salts in a range similar to the physiological concentrations,[1, 2, 7-9] the studies reported here are carried out at room temperature, without an added electrolyte, and are mainly concerned with the physical properties of micelles formed by these fascinating bio-surfactants. We include the taurine and glycine-conjugated forms of bile salt because of their prevalence in the upper intestinal tract.

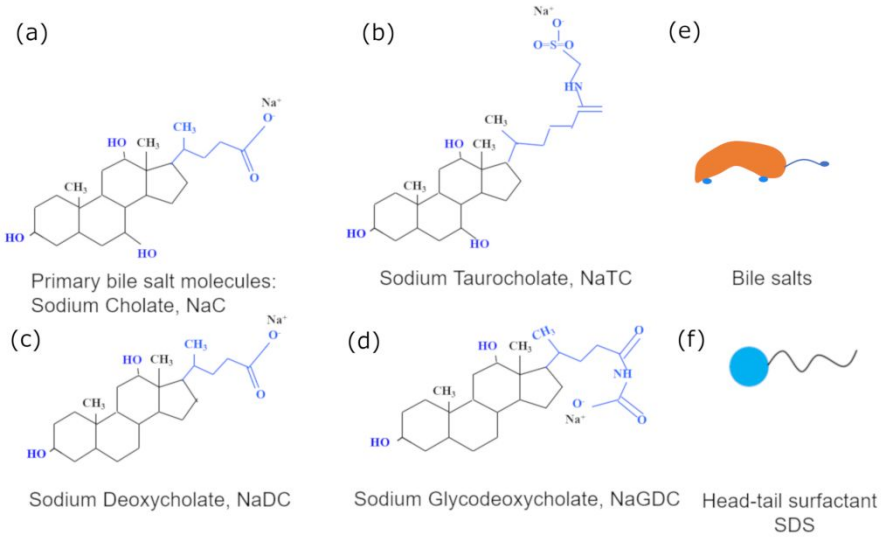

Figure 2. Chemical structure of four bile salts and schematic representation of the hydrophilic and hydrophobic regions. (a) Sodium cholate, NaC is a primary bile salt that contains three hydroxyl groups. (b) Sodium taurocholate, NaTC, a taurine conjugate of NaC, has three hydroxyl groups and is considered to be a tertiary bile salt. (c) Sodium deoxycholate, NaDC, with two hydroxyls present, is a secondary bile salt. (d) Sodium glycodeoxycholate, NaGDC, a glycine conjugate of NaDC, also contains two hydroxyl groups. (e) Schematic for the steroid structure of bile molecules, showing the few hydrophilic regions in blue and the conjugation site and the hydrophobic face. (f) Schematic for the structure of a classical head-tail surfactant with the hydrophobic tail and hydrophilic head (blue). The unusual structure of the bile salts and the specific number, orientation, and position of the hydroxy groups influence their self-assembly.

Scheludko Cell and Interferometry Digital Imaging Optical Microscopy (IDIOM) protocols: The set-up shown schematically in Figure 1b includes a thin film cell that allows the creation of a foam film of diameter 1-2 mm either using a glass tube (Schedluko-like)[35] or a porous plate (with a hole bored into it). The thin film cell is placed in a closed container with an aqueous solution added to create a saturated atmosphere and minimize the influence of evaporation and air currents.[35] First, a biconcave drop is formed within the cell, and then the liquid is slowly withdrawn using a sidearm connected to a syringe pump to create a plane-parallel film with desired size and initial thickness (<100 nm). A thicker meniscus that emulates a Plateau border surrounds the plane parallel film. The Laplace

pressure of a film in the Scheludko-like cell is estimated using $P_c \approx 4\gamma d_c / \left(d_c^2 - d_f^2\right)$, where d_c and d_f refer to cell diameter and diameter of the plane parallel film, respectively, and γ refers to the surface tension value.[35] As the capillary pressure depends upon both the film size and the cell-size, these sizes are kept similar for all stratification experiments to have a meaningful comparison.[35] The thin film is illuminated by white light, and the intensity variations within the stratifying thin film drainage are recorded with the FASTCAM Mini UX 100 high-speed camera attached to a magnification system (Navitar Zoom 6000, with added microscope objective).

Every pixel in a color image obtained by a digital camera can be read as a composite of three intensities of red (wavelength λ = 650nm), green (λ = 546nm) and blue (λ = 470nm) light, and each color channel has values in the range of 0-4095 (for RAW image with 12-bit depth). The IDIOM protocols rely on white light illumination and use digital filtering to obtain simultaneous intensity maps for three wavelengths, and consequently obtain thickness measurements, by using the interferometry equation:

$$h = \left(\frac{\lambda}{2n\pi}\right) \arcsin\left(\sqrt{\frac{\Delta}{1 + 4R(1-\Delta)/(1-R)^2}}\right) \quad (1)$$

where λ is the wavelength of light, $\Delta = \left(I - I_{\min}\right) / \left(I_{\max} - I_{\min}\right)$, and $R = \left(n-1\right)^2 / \left(n+1\right)^2$. Here I represents the intensity value measured in each pixel, $I_{\max}$ and $I_{\min}$ are the maximum and minimum intensity values, and n is the refractive index of the bulk solution. The Fresnel coefficient $R = (n-1)^2 / (n+1)^2$ is computed using the refractive index n of bulk solution (in this case, we assume n = 1.33, and hence thickness is an effective

measurement[25, 26, 29]). The image analysis is carried out in MATLAB R2015a with specially developed codes.

Thin Film Balance (TFB) method: The thin film balance for measuring disjoining pressure isotherm was first developed by Mysels and Jones[45] and was later refined by Exerowa and Scheludko.[46] The set-up used in the current study emulates the design by Dimitrova *et al*.[47] The range of pressures measured in a porous plate is set by the porosity of the fritted glass used, and in the experiments described herein, the porosity is in the range of 10-15 μm . The minimum capillary pressure ($P_c \sim 35$ Pa) is set by the size of the plane-parallel film in the Scheludko cell, but in thin film balance, P_c can be manipulated by decreasing the aspect ratio of hole depth/hole radius. The low aspect ratio is achieved by tapering the disc to create a small hole depth, as discussed by Bergeron and Radke, who were the first to measure disjoining pressure contributed by supramolecular oscillatory structural forces.[25] A hole with a diameter of 1mm was drilled at the center of the porous plate, and the porous plate cell was directly connected to a pressure transducer (Omega, PX409-001G5V) and the syringe pump. Precaution was taken to remove air bubbles in the tubes to avoid errors in the pressure measurement. The capillary pressure is varied by slowly withdrawing the liquid from the porous plate using the syringe pump. A waiting time of 10 minutes allows the film to reach equilibrium thickness (measured using IDIOM protocols) for that fixed pressure, $P_r - P_g$ registered through the pressure transducer. After carefully measuring the height difference between the pressure transducer and the film, disjoining pressure is obtained using equation (2):

$$P_c = P_g - P_l = P_g - P_r - \Delta\rho g h = \Pi \qquad (2)$$

RESULTS AND DISCUSSION

Surface tension and CMC of the four bile salts: Surface tension measurements obtained for the four bile salts using maximum bubble pressure tensiometry (MBPT) are presented in Figure 3. We characterized the dynamic adsorption and dynamic surface tension of bile salts using MBPT for the apparent surface age, t_a in the range 10 ms-10 s. [48] The apparent surface age depends on bubbling rate, whereas surface tension is computed from the maximum pressure measured in each cycle of bubble formation, growth and release. The quasi-equilibrium surface tension values shown in Figure 3, obtained by extrapolation of MBPT datasets, are comparable to those reported in the literature.[49, 50] The four bile salts reduce surface tension only marginally (in the range of 10-25 mNm^{-1}), unlike typical HT surfactants (like SDS) that reduce the surface tension of aqueous solutions by >35 mNm^{-1} for comparable concentrations (> 5 mM). We find that the maximum drop of surface tension is obtained for sodium deoxycholate, and the relative effectiveness as a surfactant decreases as follows: NaDC>NaGDC>NaC>NaTC. The overall low effectiveness of bile salts as surfactants is often linked to their peculiar steroidal structure and lack of distinct hydrophobic and hydrophilic regions. Bile salts with two hydroxyl groups (NaDC and NaGDC) appear to have higher effectiveness than those with three hydroxyl groups (NaC and NaTC). The BS equilibrium surface tension curves (see Figure 3) do not display a sharp change in slope associated with CMC for variation in surface tension (and other colligative properties) for HT surfactants like SDS,[49] and as the core of BS micelles is not completely hydrophobic, even the solubilization behavior differs from the HT surfactants. [1-15, 18-21]

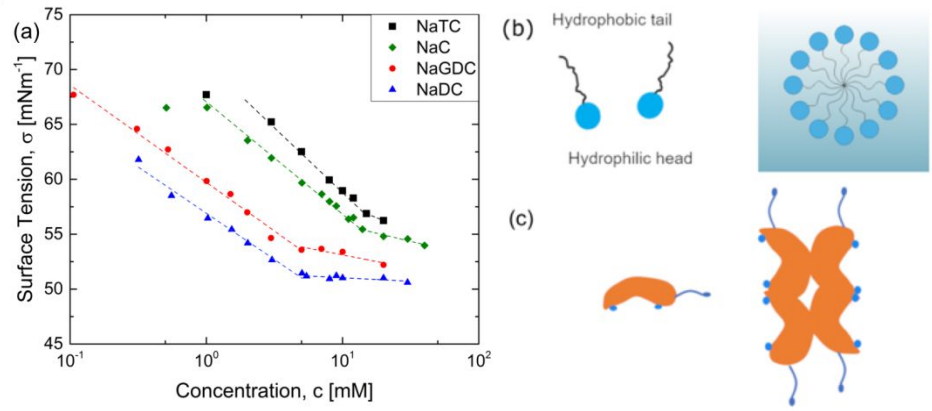

Figure 3. Surface tension of the four bile salts as a function of concentration. (a) Typically amphiphilic molecules are considered suitable surfactants if the value of surface tension decreases by 30 mNm^{-1} at a concentration of 10 mM. All bile salts are mildly surface-active, and though the surface tension values show a slope change allowing identification of CMC, the transition is not as sharp as observed by traditional head-tail surfactants. (b) Example of micellization in typical head-tail surfactant. (c) Aggregation of bile salt (and other steroidal molecules) involves fewer molecules, the higher influence of hydrophobic interactions, and higher polydispersity in shape and size.

The measured values of critical micelle concentration (CMC) are NaC (12.8 mM), NaDC (4.7 mM), NaGDC (4.7 mM), and NaTC (~15 mM) respectively (are determined here with an error < 0.5 mM). The measured values of critical micelle concentration (CMC) are in the same ball-park as the values reported in the literature using tensiometry, pyrene-based fluorescence methods, conductivity, simulations, and isothermal titration conductivity.[1-4, 7-11, 14, 15, 17, 49-56] Observed differences in the absolute values BS CMCs are attributed in the literature to sensitivity to the concentration of electrolytes and impurities, though and additional influence of pH becomes significant close to the pKa values.[15, 54-56] The surface tension data shows that the bile salts with a matched number of hydroxyl groups have similar CMC values (for example NaDC and NaGDC have two hydroxyl groups each). The BS micelles show characteristics similar to aggregates formed by small-molecular gelators,[57-60] and liquid crystal formers[61-63] (chromonics) more than HT surfactants. Simulations by Verde and Frenkel[51] show that bile micelles under

physiological conditions (0.15 NaCl) assemble and disassemble rapidly, and the free energy of disassembly at concentrations 8 times the CMC is still comparable to thermal energy. Thus micelles of BSs (under the physiological conditions) are less stable than the SDS micelles, and a relatively large fraction of dimers and monomers co-exist with larger aggregates.

Stepwise thinning of foam films formed with aqueous NaC solution: Single film drainage experiments carried out in a Schedluko-like cell reveal that the foam films made with micellar NaC solutions at 60 mM ($c/CMC \approx 4.7$) exhibit the three characteristic features of stratification: regions with distinct grayscale intensity (see Figure 4a) correlated with the underlying thickness variations (Figure 4b), and the quintessential stepwise thinning in the plot of average film thickness *vs.* time (Figure 4c). The stratification process proceeds by spontaneous nucleation and growth of thinner, darker domains, and brighter, thicker white spots (that themselves can grow, move, and coalesce) appear at the moving front between the growing thinner domain and its thicker surrounding.[29-31, 33] Quite recently, Zhang *et al.*[30] utilized IDIOM protocols to show that the white spots are relatively flat, pancake-like structures and termed these nanoscopic structures as mesas, recognizing that the thickness of such mesas is in tens of nm, even though their width is in the tens of microns. In this study, we refer to the mesas that flank the growing domains as frontal mesas, to contrast them with 'isolated mesas' that spontaneously emerge even though no moving fronts associated with domain expansion are involved. The spatio-temporally resolved thickness maps created using IDIOM protocols (see Figure 4b) reveal the coexistence of thick-thin flat regions, as well as several non-flat regions including both frontal and isolated mesas. At matched c/CMC values, the NaC films exhibit a higher

heterogeneity than observed for the salt-free SDS films (see Figure 1 for example). Both the higher thickness heterogeneity and the formation of isolated mesas are features shared with the salt-added SDS foam films.[33] Stepwise thinning, with two steps only, is observed in the plot of average thickness with time in Figure 4c for 60 mM and 100 mM NaC foam films. The step size, $\Delta h = 7.7 \pm 0.7$ nm measured for 60 mM NaC foam films, is larger than $\Delta h = 5.4 \pm 0.5$ nm measured for 100 mM films.

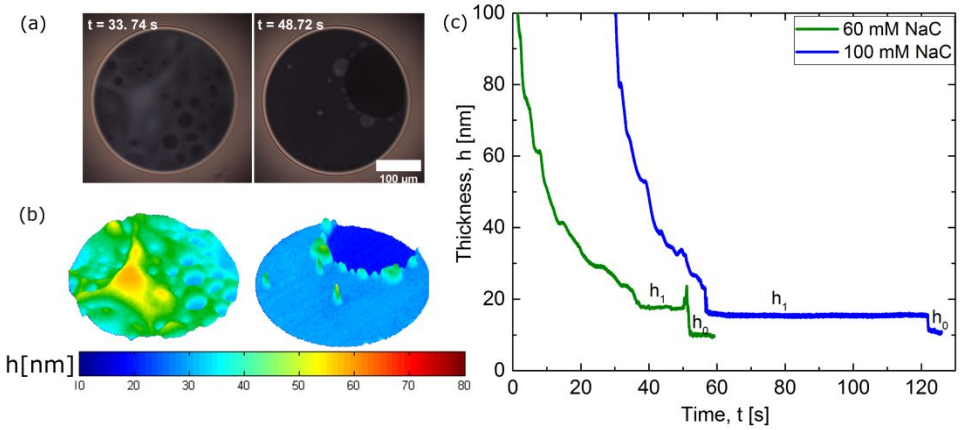

Figure 4. Drainage *via* stratification in micellar foam films of aqueous sodium cholate (NaC) solutions. (a) Two snapshots of stratifying foam films containing aqueous solutions of NaC (60 mM; $c/CMC \approx 4.7$) showcase multiple thinner darker domains and spontaneously formed white spots that flank a thinner darker domain. The scale bar corresponds to 100 µm in the plane of the film. (b) Thickness maps created using the IDIOM protocol illustrate how darker domains correspond to flat regions, whereas the white spots are pancake-like structures (hence called mesas). The color-map shows thickness values are in the nm range. (c) The evolution of average thickness with time shows only two discernible steps for the plotted for 60 mM foam films and the number of steps remains the same if the concentration is increased to 100 mM ($c/CMC \approx 7.8$). The data are shifted horizontally for the 100 mM NaC foam films to illustrate the difference in thinning behavior.

Stratification in micellar foam films made with NaDC and NaGDC solutions:

Next, we discuss stratification in foam films made with secondary bile salts: NaDC and its glycine-conjugate, NaGDC. Both have two hydroxyl groups, and in addition to the similarity in their chemical structure, both have a very similar CMC values. Figure 5

includes two gray-scale images, each for 30 mM NaDC and NaGDC (for similar values of $c/CMC \approx 6.4$) and the corresponding thickness maps. In both Figure 5a and 5b, the second, later stage snapshot shows three co-existing thickness regions: a thinner, darker domain (flat film) surrounded by the iso-intensity, brighter (hence thicker) flat film, and a set of frontal mesas near the moving front between the expanding domain and the surrounding film.

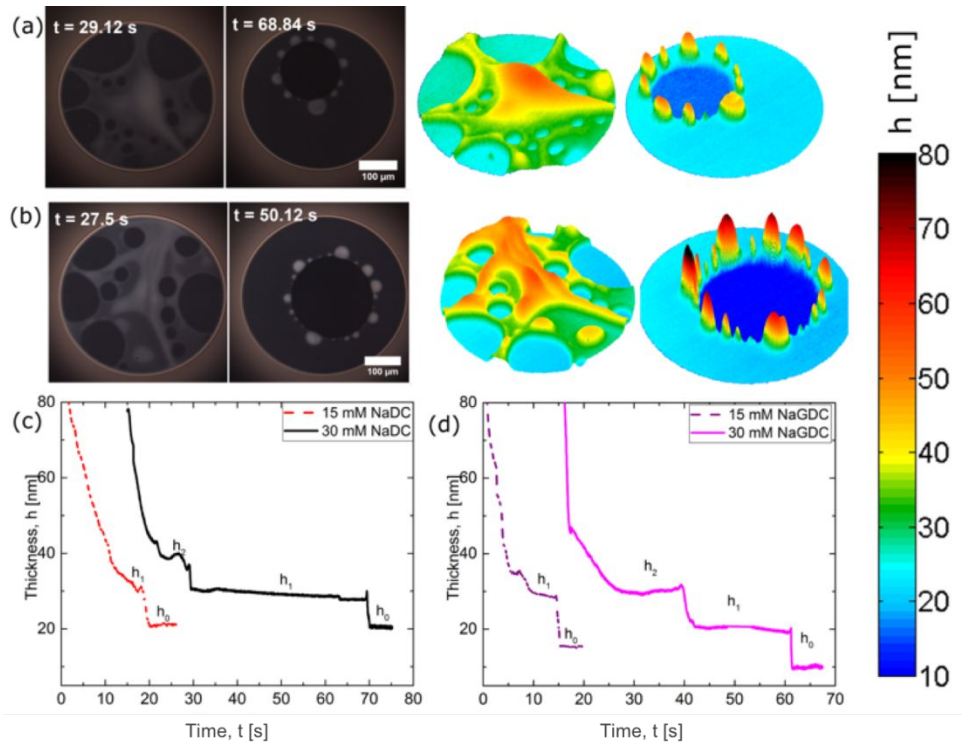

Figure 5 Stratification in foam films formed by aqueous solutions of NaDC and NaGDC, two secondary bile salts carrying two hydroxyl groups. (a) Stratification in 30 mM ($c/CMC \approx 6.4$) sodium deoxycholate (NaDC) and its thickness map obtained from IDIOM protocols. (b) Stratification in 30 mM sodium glycodeoxycholate (NaGDC) and its thickness map obtained from IDIOM protocols. The scale bar represents an in-plane length scale of 100 μm, and the color-map shows thickness in nm. (c) Evolution of average film thickness for 15 mM ($c/CMC \approx 3.2$) and 30 mM NaDC foam films showing two and three stepwise transitions, respectively. (d) Average film thickness plotted as a function of time for 15 mM and 30 mM NaGDC foam films shows a smaller final film size than observed for NaDC.

The plot of average thickness as a function of time for 15 mM NaDC film ($c/CMC \approx 3.2$, Figure 5c) shows an evidence for two layers, with a step size, $\Delta h = 10.8 \pm 0.7$ nm. On increasing the concentration to 30 mM, three layers with smaller step size, $\Delta h = 9 \pm 1$ nm can be observed. Similarly, the plot of the average thickness as a function of time for foam films made with 15 mM NaGDC reveals two layers with a step size of $\Delta h = 12.4 \pm 1$ nm, whereas films made with 30 mM NaGDC show evidence for three layers, with a smaller step size of $\Delta h = 9.6 \pm 1$ nm. Both the increase in the number of layers and the decrease in the step size on increasing surfactant concentration are features that NaDC and NaGDC foam films share with observations of classical head-tail surfactants like SDS. In contrast, the foam films formed with NaC solutions seem to exhibit only two steps in experiments carried out using the current cell and pressure ranges. Furthermore, unlike NaC foam films that show the spontaneous appearance of isolated mesas in addition to frontal mesas, NaDC and NaGDC foam films show the very pronounced manifestation of frontal mesas.

Thinning and drainage of aqueous sodium taurocholate (NaTC) solution: In Figure 6a, an image sequence shows the intensity variations (in gray scale) associated with the thickness change during drainage of a foam film formed using 80 mM NaTC (c/CMC~5). The image sequence shows the formation of multiple darker, thinner domains, as well as frontal mesas around a single domain in the last snapshot. However, the average thickness evolution plots for NaTC for 80 mM NaTC do not reveal any stepwise transitions, even though the visualization of the films shows the presence of distinct thick and thin regions. The observed behavior is reminiscent of observations for aqueous SDS foam films containing added salt (50 mM SDS + 80 mM NaCl), and the image sequence (included in

Figure 6b) shows similar thickness inhomogeneity. In a previous study focused on aqueous SDS solutions,[33] we argued that the addition of salt at a fixed surfactant concentration leads to a substantial decrease in the amplitude of the supramolecular oscillatory structural forces and a reduction in the number of thickness transitions, eventually leading to the disappearance of stratification. Indeed, the bile salt solutions consistently show thickness variations and transitions that show smaller intermicellar distances and smaller amplitude for supramolecular oscillatory structural force contributions, as discussed next.

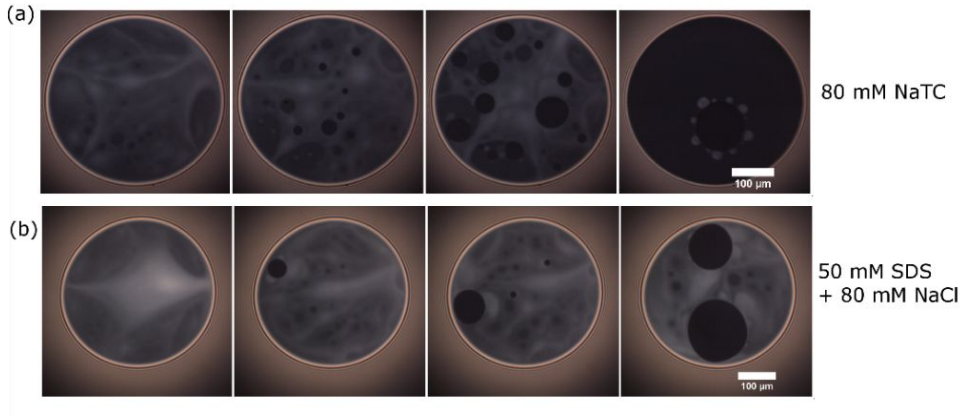

Figure 6. Image sequences contrasting the drainage behavior of micellar foam films formed by solutions of NaTC and SDS (salt added). (a) Drainage in foam films created with aqueous solutions of sodium taurocholate (NaTC) with c = 80 mM. (b) Drainage in foam film formed with SDS, with c = 50 mM SDS and added salt (80 mM NaCl). In both of these scenarios, drainage of the films proceeds with non-uniform thickness with large areas of white regions. The scale bars represent 100 μm.

Step size decreases with increasing bile salt concentration: The changes in step size with increasing concentration of NaC in Figure 7a (closed symbols) are extracted from the h_1 to h_0 transition (for the stratification process exhibits only two layers for NaC solutions). To compare with independent intermicellar measurement, we included in open symbols in Figure 7a two alternative determinations of intermicellar distance from scattering experiments.[64, 65] Zakrzewska *et al.*[65] measured intermicellar distance 7.9 ± 0.5 nm for 70 mM NaC using small-angle X-ray scattering, whereas we found a step

size of $\Delta h = 6.7 \pm 0.5$ nm using stratification experiments. For 100 mM NaC, Santhanalakshmi *et al.*[64] determined from the scattering experiment a distance of 6.28 nm, which is close to our value of 5.4 nm. In foam films made with ionic micelles, the step size is typically greater than the diameter of the micelles and the effective size of the micelles $d = 2(l_{\text{Bile Salt}} + \kappa^{-1})$ can be computed by combining molecular size with Debye length, κ^{-1}. For example, the step size $\Delta h = 7.7 \pm 0.7$ nm measured for 60 mM NaC solutions exceeds the effective size of the micelles, $d = 5.52$ nm determined by the molecular size $l_{NaC} = 1.06$ nm[64] and the concentration-dependent Debye length is $\kappa^{-1} = 1.7$ nm. For the micellar solutions, the Debye length, which includes the effect from free ions and the macroions,[66] is computed using $\kappa^2 = 8\pi l_B[\text{CMC} + (\alpha/2)(c - CMC)]$ and $l_B = e^2/\varepsilon kT$. Here, Bjerrum length, l_B = 0.72 nm in water, ε is the dielectric constant of the medium, and α is the degree of ionization. As the bile salt micelles are quite polydisperse, and the CMC is not as well-defined as for HT surfactants, the estimate is less reliable than for SDS, though clearly the step size is not equal to the effective size (in aggreement with SDS datasets).

A close inspection of the step-size *vs.* concentration data shown in Figure 7b shows that the trihydroxy bile salts display a smaller step size than dihydroxy bile salts, implying either intermicellar distance, or micelle size, or both could be smaller. The step size variation for foam films formed with NaGDC and NaDC displays the $\Delta h \sim c^{-1/3}$ power law behavior as shown in Figure 7b. The concentration-dependent decrease in step size emulates the scaling law observed for classical ionic surfactants[23, 24, 30] like SDS and nanoparticles under confinement.[22, 28, 67] The usual $\Delta h \sim c^{-1/3}$ power law is considered to

be a manifestation of the dependence of intermicellar distance on the number density of micelles or particles.[22-24, 28, 67] However, the variation of step size with concentration displayed by NaC is quite unusual ($\Delta h \sim c^{-4/5}$) and has not been reported before. A plausible explanation for the unusual concentration dependence might be the following. The step size for NaC micellar foam films is extracted from the transition from h_1 to h_0, and as both DLVO forces and supramolecular oscillatory structural forces could contribute to this film thickness range as discussed in a subsequent section.

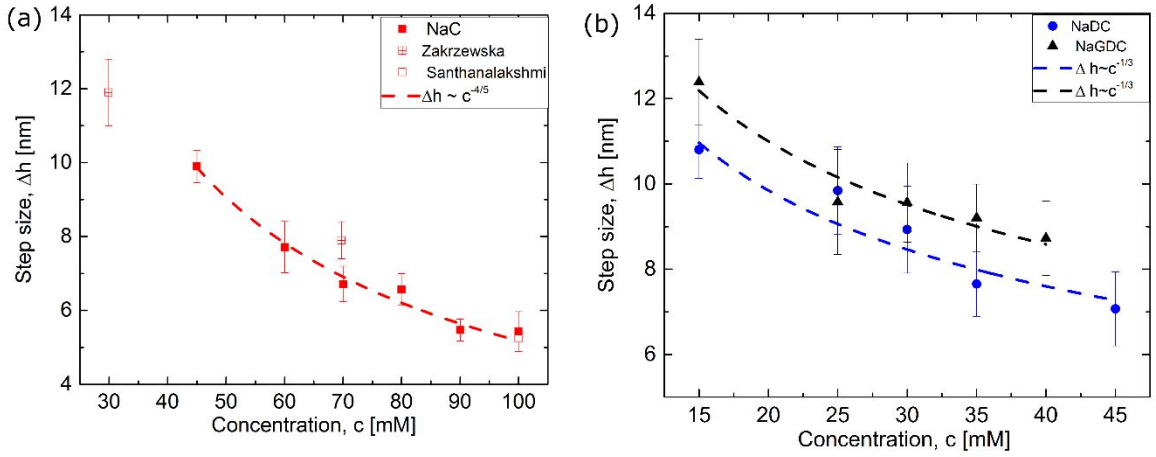

Figure 7. Concentration-dependent variation in step size. (a) Measured step size values (closed symbols) as a function of concentration for NaC foam films show $\Delta h \sim c^{-4/5}$ dependence (dotted line). Intermicellar distance values obtained from scattering experiments by Zakrzewska[65] and Santhanalakshmi[64] are shown in open symbols. (b) Step size *vs.* concentration data for NaDC and NaGDC films follow $\Delta h \sim c^{-1/3}$ dependence (dotted lines), similar to those obtained from stratifying SDS foam films.

Disjoining pressure of bile salts: measurements and theory. The Laplace pressure that acts on the foam film is varied by gradually varying the area of the plane-parallel film as shown in Figure 8a, and the counterbalancing thickness-dependent disjoining pressure (see Figure 8b) is then measured using Thin Film Balance (TFB) technique. Each data point reported for 30 mM NaDC foam films in Figure 8b is obtained

by waiting for local equilibrium. For example, the five different film sizes in the snapshots shown in Figure 8a correspond to the indicated five points for disjoining pressure in Figure 8b. The corresponding thickness maps shown in Figure 8c illustrate that the thickness of the entire film is uniform for the corresponding measurement.

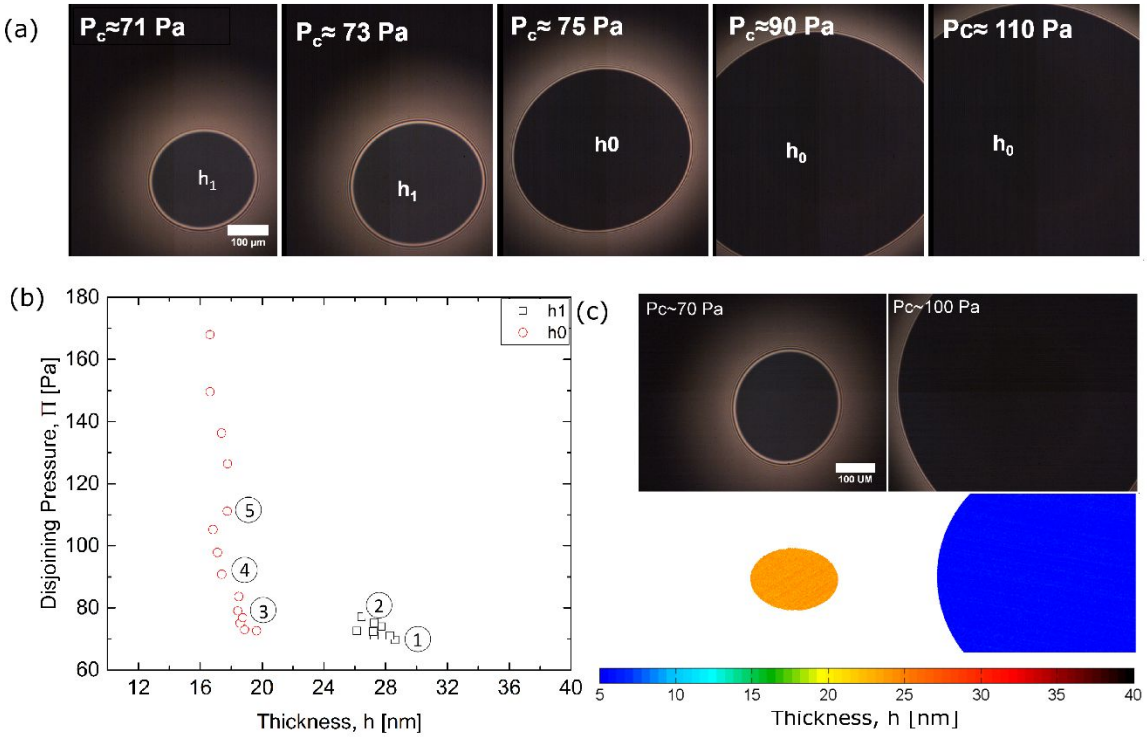

Figure 8. Disjoining pressure measured from thin film pressure balance for NaDC foam films. (a) Variation in pressure and film size at each metastable thickness. (b) Experimentally measured equilibrium disjoining pressure data obtained from thin film pressure balance method for 30 mM NaDC foam films. (c) Snapshots and the corresponding thickness maps at the transition between thickness branches.

Three thickness steps are observed experimentally for 30 mM NaDC films. However, since the transition from h_2 to h_1 occurs too rapidly to make an equilibrium measurement, only two metastable branches of the disjoining pressure isotherm are shown. The transition from one branch to another, say from h_1 to h_0 in 30 mM NaDC foam films, can be triggered by changing film area or applied pressure. In this case, once the maximum pressure reaches 75 Pa, the film thickness transits into the next layer *via* nucleation and

growth of thinner, darker domains. The period of the oscillation in the measured disjoining pressure is around 8 nm, which is close to the step size found from the dynamic stratification experiments by plotting thickness versus time. The disjoining pressure reported by Zhang and Sharma for 50 mM SDS foam films, (same *c*/CMC value as 30 mM NaDC) foam films show a much larger amplitude (200 Pa) and larger oscillation frequency (13 nm) correlating with larger step size, micelle size and intermicellar distance. Moreover, 50 mM SDS films have four layers during stratification, whereas 30 mM NaDC films have three layers. Lower amplitude, smaller step size, and lower number of steps in NaDC films further confirm that NaDC micelles have weaker interactions than the SDS micelles.

The experimental measurement of disjoining pressure in Figure 8b requires a considerable amount of time and effort and represents one of the countable few measurements ever reported for ionic micellar fluids.[25, 31] The primary difficulty lies in obtaining a homogeneous film thickness in the entire film for long enough at each value of Laplace pressure. These conditions are not met easily as perturbations lead to the nucleation of progressively thinner domains. For example, withdrawing the fluid from foam film to change Laplace pressure using syringe pump for the NaC foam films or films made with SDS with added salt rupture relatively quickly. Many researchers[31-33, 43, 68-71] (including the coauthors) utilize theoretical expressions for supramolecular oscillatory structural forces contributed by confinement induced-layering of monodisperse charged spheres including ionic micelles (SDS) to get a better understanding of the stratification process. The magnitude, oscillation period, and decay length of supramolecular oscillatory contribution to disjoining pressure for micellar solutions of typical ionic surfactants can be described using the following phenomenological expression[33]

$$\Pi_{os} = \rho f(\varphi) k_B T \cos(\frac{2\pi h}{\Delta h}) \exp[((\frac{d}{\Delta h})^3 - \frac{h}{\Delta h}) g(\varphi)] \quad (3a)$$

$$f(\varphi) = \frac{\left(1+\varphi+\varphi^2-\varphi^3\right)}{(1-\varphi)^3}; g\left(\varphi\right) = \frac{\sqrt{2/3} + a_1 \Delta\varphi + a_2 (\Delta\varphi)^2}{\left(b_1/\Delta\varphi\right) - b_2} \quad (3b)$$

Here the effective volume fraction of the micelles $\varphi = \rho\pi d^3/6$ is computed based on $d = 2(R+\kappa^{-1})$, $\Delta\varphi = \pi/3\sqrt{2} - \varphi$, the compressibility factor $f\left(\varphi\right)$ is defined using the Carnahan-Starling formula, and the values $a_1 = 0.24, a_2 = 0.63, b_1 = 0.49, b_2 = 0.42$ are obtained from the calculations by Kralchevsky and Denkov.[68] The prefactor $\rho f(\varphi) k_B T$ is related to the amplitude of the disjoining pressure. Here ρ is the number density of micelles, $\rho = (c - \mathrm{CMC}) N_A / N_{agg}$ and k_B is the Boltzmann constant. However, the phenomenological expressions for supramolecular oscillatory structural forces given in equation 1 (and similar expressions in literature[68, 69]) are quite unsuitable for describing the behavior of bile salt solutions. The values of CMC and the transition at CMC are not as sharply defined as for the SDS system, and the estimation of the number density of micelles, compressibility factor, and decay factor must account for the unknown polydispersity in shape and size of bile micelles. The previous attempts that model the influence of polydispersity[72, 73] on the interaction between colloidal spheres show that polydispersity lowers the amplitude of disjoining pressure. Lower amplitude of disjoining pressure can qualitatively explain the observations of less sharp and fewer thickness transitions, the formation of isolated mesas, and the disappearance of the diffusive regime during the domain growth.

The step-sizes obtained for bile salts appear to be relatively small compared to those obtained for SDS micelles. Even at 100 mM, the SDS solutions exhibit a larger step size than measured for the entire range of bile salt concentrations. We postulated earlier that the unexpected concentration variation of step-size observed for NaC (power law of $c^{-4/5}$) could result from the possibility that the equilibrium film thicknesses h_0 and h_1 are in the range where both DLVO forces and supramolecular oscillatory structural forces can act together. Since the bile micelles have a smaller micelle size (due to smaller aggregation number), the value of h_0 is more likely to be influenced by electrostatic double layer forces than the corresponding values for SDS solutions. To elucidate the role of the two DLVO forces, (van der Waals, attractive and electrostatic double layer forces, repulsive), we plot the computed value of each thickness-dependent contribution to disjoining pressure for 60 mM SDS foam films, and also include supramolecular oscillatory structure force contribution computed using expression 1. The van der Waals contribution can be computed using $\Pi_{VW} = A/6\pi h^3$ where A is the Hamaker's constant. The electrostatic diffuse double layer forces are calculated by using the following expression:

$$\Pi_{el} = 64nkT\frac{\exp\left(e\phi_0/2k_BT\right)-1}{\exp\left(e\phi_0/2k_BT\right)+1}\exp\left(-\kappa h\right) \qquad (4)$$

Here n is the number density of ions, e is the elementary charge, and ϕ_0 is the surface potential. Contributions by van der Waals attraction (black dashed line), electrostatic diffuse double layer forces (red line), and supramolecular oscillatory structural forces (blue line) are also shown in Figure 9a. The supramolecular oscillatory structural forces much longer ranged than the double layer forces and van der Waals forces. Still, close

examination of Figure 9a presents a strong argument in favor of the influence of electrostatic diffuse double layer forces for SDS solutions. Indeed, we find (see Figure 9b) that the final film thickness h_0 data plotted against the total electrolyte concentrations I = CMC + $(\alpha/2)(c - CMC)$] for SDS, NaC, and NaDC follows the same $h_0 \sim I^{-1/2}$ power law as displayed by Debye length.

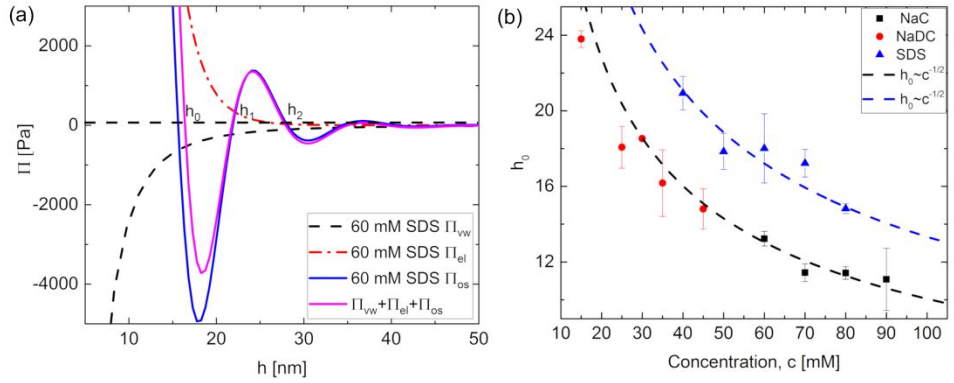

Figure 9. **Concentration-dependent variation in final film thickness and thickness-dependent variation in disjoining pressure.** (a) Various contributions to disjoining pressure variation with thickness are shown for 60 mM SDS foam films. The intersection of applied Laplace pressure (horizontal dashed line) with total disjoining pressure leads to the three metastable thicknesses indicated on the curve. (b) Final film thickness h_0 variation with concentration for NaC, NaDC, and SDS foam films.

Topography of foam films formed with micellar solutions of bile salts: Two thickness maps, created using IDIOM for foam films containing bile salts at the same relative concentration above CMC, are shown in Figure 10. Both NaC and NaTC, bile salts with three hydroxyl groups, appear to have smaller step sizes and smaller final film thickness than NaDC and NaGDC. Both NaC and NaTC show the formation of thinner, darker domains flanked by frontal mesas. Thus, it appears that the bile salts with a similar number of hydroxyl groups stratify in a similar fashion. The frontal mesas in the thickness map for NaTC are distributed relatively uniformly but have a distinct variation in size and shape of mesas, which mimic the shape variations in mesas formed in stratifying micellar

SDS films (see Zhang and Sharma,[32] for details). Thus the interaction between bile molecules is not as strong as classical head-tail surfactants such as SDS, and the micelles are relatively less stable. Indeed, the lower number of thickness transitions, a higher number of isolated mesas and absence of domain expansion regime without frontal mesas are all consistent with lower amplitude of supramolecular structural forces for bile salts if contrasted with salt-free aqueous SDS micellar solutions. The diminished amplitude of disjoining pressure on the addition of salt for SDS micelles yields the same kind of differences as observed on contrasting NaDC and NaGDC with NaC and NaTC (the latter emulate high salt, lowest amplitude disjoining pressure case).

In micellar foam films formed with salt-free aqueous SDS solutions, the initial domain expansion occurs without mesas or white spots present, leading to an overwhelming focus on domain expansion dynamics without mesas present.[22-24, 70, 71] Such models provide little insight into stratification in bile salts, as mesas seem to appear almost concurrently with the appearance of thinner, darker domains. In the recently introduced comprehensive theoretical approach from Zhang and Sharma,[29-31] the observed domain expansion dynamics, the formation of the nanoridge as well as frontal and isolated mesas follows from a nonlinear thin film model that explicitly accounts for the role of supramolecular oscillatory structural forces. The ease of formation of frontal mesas for all bile salts thus itself suggests that the amplitude of supramolecular structural forces is relatively mild compared to the salt-free, aqueous micellar SDS solutions. We find that the nanoscopic topographical features visualized with IDIOM protocols for bile salts emulate the features observed in micellar aqueous SDS solutions with added salt, implying that the

supramolecular structural forces have fewer oscillations and weaker magnitude that salt-free SDS aqueous solutions.

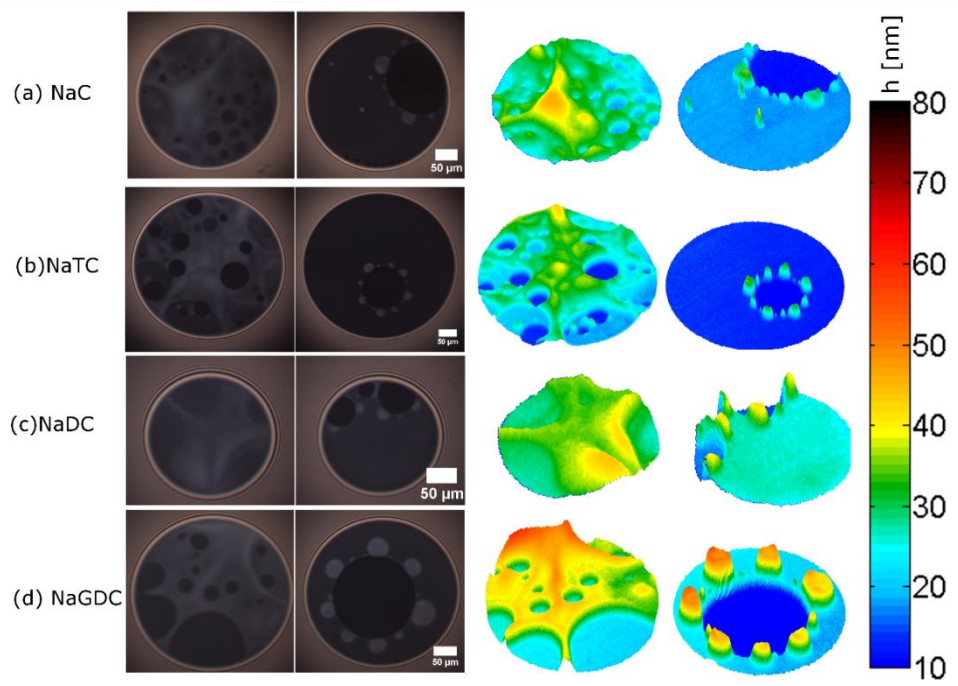

Figure 10 Comparison in stratification in different bile salts carries out at the matched value of *c*/*CMC*. (a) NaC, 60 mM; (b) NaTC, 80 mM; (c) NaDC, 25 mM NaDC and (d) NaGDC 25 mM.

CONCLUSIONS

In this study, we present clear evidence for stratification in foam films made with aqueous micellar solutions of four different bile salts (BS). We visualize and characterize stepwise thinning, nanoscopic topography, concentration-dependent variation of step-size and number of steps, and stability of BS foam films. The foam films made with aqueous solutions NaC, (a primary bile salt) exhibit stratification with at most two thicknesses manifested, whereas the secondary bile salts NaDC and its glycine conjugate form, NaGDC exhibit more steps. The drainage of foam films containing bile salts with three hydroxy groups, including the primary bile salt NaC and its taurine conjugate NaTC, a tertiary bile salt, is qualitatively similar to the behavior of SDS films with salt added to surfactant

solution. Stratification in NaDC and NaGDC foam films is similar to that observed in low concentration SDS micellar foam films (in the absence of added salt). An increase in the surfactant concentration results in an increase in the number of layers in NaDC and NaGDC, however, the number of layers in NaC foam films remains constant. We observed that the frontal mesas form some after a domain appears, unlike salt-free SDS solutions that display a pronounced diffusive growth regime, here only the constant velocity mode is observed. Stratifying BS foam films of bile salt exhibit features that are consistent with the observations made for salt-added SDS solutions and can be attributed to the relatively low amplitude of supramolecular oscillatory structural forces. However, as the micellar bile system is highly polydisperse, thus the phenomenological model of supramolecular oscillatory structural forces for the monodisperse system needs revision.

The measured step size exhibits a $\Delta h \sim c^{-1/3}$ power law behavior for NaDC and NaGDC films, which was previously observed for foam films containing spherical micelles. However, NaC step size shows a $\Delta h \sim c^{-4/5}$ power law, which has not been reported before. We measured disjoining pressure isotherm for 30 mM NaDC (~6CMC) using thin film balance. However, only data from two branches is measurable and the maximum pressure measured for these films with two layers with lower amplitude than 50 mM SDS (~6CMC) films. This confirmed that intermolecular and surface forces are not as strong for bile salts as for classical SDS molecules. The NaC foam films are even less stable than NaDC foam films, thus it is hard to measure disjoining pressure experiment successfully.

The possibility of characterizing drainage *via* stratification of foam films containing BS micelles opens up the possibility of utilizing thin film studies for examination of intermicellar interactions and supramolecular oscillatory structural force contribution to

disjoining pressure. We find that the BS foam films have far fewer transitions that observed for micellar SDS solutions and other micellar HT surfactant solutions, that are contributed by weaker intermicellar interactions as well as faster decay of oscillatory structural forces. Few transitions imply that BS films are likely to rupture in shorter times. The bile salts with three hydroxyl groups have higher CMC and fewer stepwise transitions that two hydroxyl group BS, and thus we find small chemical differences influence both micelle formation and intermicellar interactions. Smaller aggregation numbers, polydispersity in size, and smaller micellar sizes, both before and after solubilization helps bile salts in physiological functions that involve transport across intestinal walls and biological membranes. We anticipate applying our technique to further study the interactions and size of combination of bile salt-bile salt, bile-salt cholesterol, and bile salt-lipid systems. We present the stratification studies of foam films formed with the bile salts with the keen awareness that foam-film based studies offer unexplored opportunities for investigating structure and interactions in mixed bile micelles, with direct relevance to their solubilization, regulatory, and drug delivery functions.

ACKNOWLEDGEMENTS

VS would like to acknowledge funding from the National Science Foundation (NSF CBET 1806011) and the initial funding support by the College of Engineering and the Department of Chemical Engineering at the University of Illinois at Chicago. VS thanks Prof. Cynthia Jamieson, UIC, and Dr. Samanvaya Srivastava, UCLA, for close reading of the manuscript and acknowledges students in the ODES-lab, especially Chrystian Ochoa, for insightful questions and comments, and Carina Martinez and Jasmine Villegas for checking and repeating surface tension measurements with bile salt solutions. SY also acknowledges the Chemistry department at UIC for funding her as a teaching assistant. SY is now employed in Abbot, Camila works at Abbvie and Jasmine is pursuing Ph. D. at University of Washington.

REFERENCES

1. A. F. Hofmann and L. R. Hagey, *J. Lipid Res.*, 2014, **55**, 1553-1595.
2. A. Macierzanka, A. Torcello-Gómez, C. Jungnickel and J. Maldonado-Valderrama, *Adv. Colloid Interface Sci.*, 2019, 102045.
3. B. Mukherjee, A. A. Dar, P. A. Bhat, S. P. Moulik and A. R. Das, *RSC Advances*, 2016, **6**, 1769-1781.
4. L. Galantini, M. C. di Gregorio, M. Gubitosi, L. Travaglini, J. V. Tato, A. Jover, F. Meijide, V. H. S. Tellini and N. V. Pavel, *Curr. Opi. Colloid Interface Sci.*, 2015, **20**, 170-182.
5. J. Maldonado-Valderrama, P. Wilde, A. Macierzanka and A. Mackie, *Adv. Colloid Interface Sci.*, 2011, **165**, 36-46.
6. P. Portincasa, A. Moschetta and G. Palasciano, *The Lancet*, 2006, **368**, 230-239.
7. A. F. Hofmann, *Physiology*, 1999, **14**, 24-29.
8. A. F. Hofmann and K. J. Mysels, *Colloids and Surfaces*, 1987, **30**, 145-173.
9. M. C. Carey, D. M. Small and C. M. Bliss, *Ann. Rev. Physiology*, 1983, **45**, 651-677.
10. D. M. Small, P. P. Nair and D. Kritchevsky, *P. P. Nair, D. Kritchevsky (Eds.)*, 1971, **1**, 249-356.
11. A. F. Hofmann and D. M. Small, *Ann. Rev. Medicine*, 1967, **18**, 333-376.
12. R. Holm, A. Müllertz and H. Mu, *Int. J. Pharm.*, 2013, **453**, 44-55.
13. Y. S. R. Elnaggar, *Inter. J. Nanomedicine*, 2015, **10**, 3955.
14. M. C. di Gregorio, L. Travaglini, A. Del Giudice, J. Cautela, N. V. Pavel and L. Galantini, *Langmuir*, 2018.
15. D. Madenci and S. U. Egelhaaf, *Cur. Opin. Colloid Interface Sci.*, 2010, **15**, 109-115.
16. H. Sugioka and Y. Moroi, *Biochim Biophys Acta Lipids m*, 1998, **1394**, 99-110.
17. K. Matsuoka and Y. Moroi, *Biochim Biophys Acta Mol Cell Biol Lipids*, 2002, **1580**, 189-199.
18. N. Funasaki, M. Fukuba, T. Kitagawa, M. Nomura, S. Ishikawa, S. Hirota and S. Neya, *J. Phys. Chem. B*, 2004, **108**, 438-443.
19. H. Sugioka, K. Matsuoka and Y. Moroi, *J. Colloid Interface Sci.*, 2003, **259**, 156-162.
20. D. Fennell Evans and H. Wennerström, *The Colloidal Domain: Where Physics, Chemistry, Biology, and Technology Meet*, Wiley-VCH: New York, 2nd edn., 1999.
21. J. N. Israelachvili, *Intermolecular and Surface Forces*, Academic Press, 3rd edn., 2011.
22. A. D. Nikolov, D. T. Wasan, P. A. Kralchevsky and I. B. Ivanov, *Ordered structures in thinning micellar foam and latex films*, World Scientific, Singapore, 1988.
23. A. D. Nikolov and D. T. Wasan, *J. Colloid Interface Sci.*, 1989, **133**, 1-12.
24. A. D. Nikolov, P. A. Kralchevsky, I. B. Ivanov and D. T. Wasan, *J. Colloid Interface Sci.*, 1989, **133**, 13-22.
25. V. Bergeron and C. J. Radke, *Langmuir*, 1992, **8**, 3020-3026.
26. V. Bergeron, A. I. Jimenez-Laguna and C. J. Radke, *Langmuir*, 1992, **8**, 3027-3032.
27. A. A. Sonin and D. Langevin, *Europhys. Lett.*, 1993, **22**, 271.

28. S. E. Anachkov, K. D. Danov, E. S. Basheva, P. A. Kralchevsky and K. P. Ananthapadmanabhan, *Adv. Colloid Interface Sci.*, 2012, **183**, 55-67.
29. Y. Zhang and V. Sharma, *Soft Matter*, 2015, **11**, 4408-4417.
30. Y. Zhang, S. Yilixiati, C. Pearsall and V. Sharma, *ACS Nano*, 2016, **10**, 4678-4683.
31. Y. Zhang and V. Sharma, *Langmuir*, 2018, **34**, 1208-1217.
32. Y. Zhang and V. Sharma, *Langmuir*, 2018, **34**, 7922–7931.
33. S. Yilixiati, R. Rafiq, Y. Zhang and V. Sharma, *ACS Nano*, 2018, **12**, 1050-1061.
34. S. Yilixiati, E. Wojcik, Y. Zhang and V. Sharma, *MSDE*, 2019, **4**, 626-638.
35. A. Sheludko, *Adv. Colloid Interface Sci.*, 1967, **1**, 391-464.
36. K. J. Mysels, S. Frankel and K. Shinoda, *Soap films: Studies of their Thinning and a Bibliography*, Pergamon Press, 1959.
37. E. S. Johonnott, *Philosophical Magazine Series 6*, 1906, **11**, 746-753.
38. V. Bergeron, *J. Phys.: Condens. Matter*, 1999, **11**, R215-R238.
39. B. V. Derjaguin, N. V. Churaev and V. M. Muller, *Surface Forces*, Springer, New York, 1987.
40. B. V. Derjaguin and A. S. Titievskaya, *Prog. Surf. Sci.*, 1992, **40**, 64-73.
41. B. V. Derjaguin, A. S. Titijevskaia, I. I. Abricossova and A. D. Malkina, *Discuss. Faraday Soc.*, 1954, **18**, 24-41.
42. J. Israelachvili and M. Ruths, *Langmuir*, 2013, **29**, 9605-9619.
43. N. C. Christov, K. D. Danov, Y. Zeng, P. A. Kralchevsky and R. von Klitzing, *Langmuir*, 2009, **26**, 915-923.
44. R. F. Tabor, H. Lockie, D. Y. C. Chan, F. Grieser, I. Grillo, K. J. Mutch and R. R. Dagastine, *Soft Matter*, 2011, **7**, 11334-11344.
45. K. J. Mysels and M. N. Jones, *Discuss. Faraday Soc.*, 1966, **42**, 42-50.
46. D. Exerowa and A. Scheludko, *CR Acad Bulg Sci*, 1971, **24**, 47-50.
47. T. D. Dimitrova, F. Leal-Calderon, T. D. Gurkov and B. Campbell, *Langmuir*, 2001, **17**, 8069-8077.
48. C. A. U. Ortiz, University of Illinois at Chicago, 2017.
49. C. J. O'Connor, B. T. Ch'ng and R. G. Wallace, *J. Colloid Interface Sci.*, 1983, **95**, 410-419.
50. C. J. O'Connor and R. G. Wallace, *Adv. Colloid Interface Sci.*, 1985, **22**, 1-111.
51. A. V. Verde and D. Frenkel, *Soft Matter*, 2010, **6**, 3815-3825.
52. A. Maestre, P. Guardado and M. L. Moyá, *J. Chem. Eng. Data*, 2014, **59**, 433-438.
53. A. Coello, F. Meijide, E. R. Núñez and J. V. Tato, *J. Pharm. Sci.*, 1996, **85**, 9-15.
54. S. Reis, C. G. Moutinho, C. Matos, B. de Castro, P. Gameiro and J. L. Lima, *Anal. Biochem.*, 2004, **334**, 117-126.
55. J. P. Kratohvil, *Adv. Colloid Interface Sci.*, 1986, **26**, 131-154.
56. A. Roda, A. F. Hofmann and K. J. Mysels, *J. Biol. Chem.*, 1983, **258**, 6362-6370.
57. P. Terech and R. G. Weiss, *Chem. Rev.*, 1997, **97**, 3133-3160.
58. P. Terech, S. Dourdain, S. Bhat and U. Maitra, *J. Phys. Chem. B*, 2009, **113**, 8252-8267.
59. K. J. Skilling, F. Citossi, T. D. Bradshaw, M. Ashford, B. Kellam and M. Marlow, *Soft Matter*, 2014, **10**, 237-256.

60. M. Zhang, S. Strandman, K. C. Waldron and X. Zhu, *J. Mater. Chem. B*, 2016, **4**, 7506-7520.
61. J. Lydon, *Curr. Opin. Colloid Inter. Sci.*, 2004, **8**, 480-490.
62. K. Nayani, R. Chang, J. Fu, P. W. Ellis, A. Fernandez-Nieves, J. O. Park and M. Srinivasarao, *Nature Comm.*, 2015, **6**, 8067.
63. J. Lydon, *J. Mater. Chem.*, 2010, **20**, 10071-10099.
64. J. Santhanalakshmi, G. S. Lakshmi, V. K. Aswal and P. S. Goyal, *J. Chem. Sci.*, 2001, **113**, 55.
65. J. Zakrzewska, V. Markovic, D. Vucelic, L. Feigin, A. Dembo and L. Mogilevsky, *J. Physical Chemistry*, 1990, **94**, 5078-5081.
66. B. Beresford-Smith, D. Y. C. Chan and D. J. Mitchell, *J. Colloid Interface Sci.*, 1985, **105**, 216-234.
67. R. von Klitzing, E. Thormann, T. Nylander, D. Langevin and C. Stubenrauch, *Adv. Colloid Interface Sci.*, 2010, **155**, 19-31.
68. P. A. Kralchevsky and N. D. Denkov, *Chem. Phys. Lett.*, 1995, **240**, 385-392.
69. A. Trokhymchuk and D. Henderson, *Curr. Opin. Colloid Interface Sci.*, 2015, **20**, 32-38.
70. J. Lee, A. Nikolov and D. Wasan, *Langmuir*, 2016, **32**, 4837-4847.
71. J. Lee, A. Nikolov and D. Wasan, *J. Colloid Interface Sci.*, 2017, **496**, 60-65.
72. R. J. Baxter, *J. Chemical Physics*, 1970, **52**, 4559-4562.
73. X. L. Chu, A. D. Nikolov and D. T. Wasan, *Langmuir*, 1996, **12**, 5004-5010.